



HAL
open science

General Expression for the Size-Dependent Optical Properties of Quantum Dots

Tangi Aubert, Aleksandr Golovatenko, Margarita Samoli, Laurent Lermusiaux, Thomas Zinn, Benjamin Abécassis, Anna Rodina, Zeger Hens

► **To cite this version:**

Tangi Aubert, Aleksandr Golovatenko, Margarita Samoli, Laurent Lermusiaux, Thomas Zinn, et al.. General Expression for the Size-Dependent Optical Properties of Quantum Dots. *Nano Letters*, 2022, 22 (4), pp.1778-1785. 10.1021/acs.nanolett.2c00056 . hal-03683852

HAL Id: hal-03683852

<https://hal.umontpellier.fr/hal-03683852v1>

Submitted on 21 Nov 2022

HAL is a multi-disciplinary open access archive for the deposit and dissemination of scientific research documents, whether they are published or not. The documents may come from teaching and research institutions in France or abroad, or from public or private research centers.

L'archive ouverte pluridisciplinaire **HAL**, est destinée au dépôt et à la diffusion de documents scientifiques de niveau recherche, publiés ou non, émanant des établissements d'enseignement et de recherche français ou étrangers, des laboratoires publics ou privés.



Distributed under a Creative Commons Attribution - NoDerivatives 4.0 International License

A general expression for size quantization in colloidal quantum dots

Tangi Aubert^{1,2}, Aleksandr A. Golovatenko³, Margarita Samoli¹, Laurent Lermusiaux⁴, Thomas Zinn⁵, Benjamin Abecassis⁴, Anna V. Rodina^{3,*}, Zeger Hens^{1,*}

¹ Department of Chemistry, Ghent University, 9000 Ghent, Belgium.

² ICGM, Univ Montpellier, CNRS, ENSCM, 34000 Montpellier, France.

³ Ioffe Institute, Russian Academy of Sciences, 194021 St. Petersburg, Russia.

⁴ Univ. Lyon, ENS de Lyon, CNRS, Laboratoire de Chimie, 69342 Lyon, France

⁵ ESRF – The European Synchrotron, 38043 Grenoble, France.

* email: anna.rodina@mail.ioffe.ru, zeger.hens@ugent.be

Abstract

While initial theories on quantum confinement in colloidal quantum dots (QDs) led to analytical band-gap/size relations, numerical methods turned out to be more accurate to describe size quantization. However, to obtain reliable sizing functions, researchers fit experimental band-gap/size datasets using models with redundant, physically meaningless parameters that break down upon extrapolation. Here, we propose a new analytical band-gap/size relation based on a proportional correction for non-parabolic bands. Using known bulk semiconductor parameters, we accurately predict size quantization for group IV, III-V, II-VI, IV-VI and metal halide perovskite semiconductors, including straightforward adaptations for negative-gap semiconductors and non-spherical QDs. Refinement with respect to experimental data is possible using the Bohr diameter as a fitting parameter, which was used to identify a statistically relevant difference in band-gap/size relation for wurtzite and zinc blende CdSe. The generic sizing function proposed here should unify QD size calibration, and enable researchers to assess bulk semiconductor parameters and predict size quantization in unexplored materials.

Size quantization in semiconductor nanocrystals or quantum dots (QDs) is often introduced by means of sizing functions, such as the equations proposed by Efros and Efros, and Brus, which express the band gap as a function of the QD size using characteristic properties of the bulk semiconductor¹⁻³. While conceptually appealing, such analytical sizing functions have been replaced for many years by more accurate, numerically-calculated relations based on effective mass or atomistic methods. However, the use of band gap/size relations in QD research goes well beyond the assessment of theoretical models on size quantization. Advanced methods for QD synthesis, studies on nucleation and growth, quantitative optical spectroscopy on QDs, the formation and simulation of QD-based devices or the assessment of QD toxicity all require accurate QD size or concentration determination. Sizing QDs by direct imaging using transmission electron microscopy (TEM) is time-consuming and can be difficult for QDs smaller than 5 nm which lack image contrast. The more convenient method derives the mean QD diameter from the size-dependent optical band gap of a QD sample, which can be obtained within minutes using a routine UV-vis spectrometer. Nowadays, calibration or sizing curves that allow calculating sizes from band gaps are available for a wide range of QDs, often in good agreement with numerically calculated relations.

These sizing curves have been established by interpolating experimental band gap/size datasets using polynomial functions with up to five fitting parameters^{4,5}, or by adding a size-dependent function, such as the inverse of a 2nd order polynomial, to the bulk band-gap energy (E_g), see Supporting Information, Section S1⁶⁻⁹. These mathematical formulas can give excellent fits to a given band gap/size dataset, as previously reported for cadmium⁴⁻⁷ and lead^{8,9} chalcogenide QDs, but a variety of other formulas do so as well (Supporting Information, Section S1). However, extrapolations based on these sizing curves can differ wildly, yielding highly unphysical results, and fitting parameters have no obvious relation to the properties of the corresponding bulk semiconductor. Hence, even after 40 years of QD

research, there is a need for an analytical sizing function that relates the QD band gap and size in terms of meaningful parameters and allows for extrapolating the experimental dataset at hand.

Here, we propose a new, semi-empirical expression to describe size quantization for a broad range of semiconductor QDs through a single fitting parameter. The gist of our approach is a correction of the impact of non-parabolic energy bands on the QD band gap. By testing the resulting sizing curve for CdX and PbX (X=S,Se), we can relate the fitting parameter to bulk semiconductor characteristics. The resulting parameter-free sizing function yields an excellent prediction of size-quantization in additional II-VI (CdTe, HgTe), III-V (InP), IV (Si) groups and metal halide perovskite (CsPbBr₃) QDs. In the case of PbTe, the prediction deviates somewhat from experimental data. Since such deviations may arise from ill-known Bohr diameters, we propose a generic function to fit band gap/size datasets using the Bohr diameter as the sole adjustable parameter. This semi-empirical sizing function can unify QD size calibration, and enable researchers to assess bulk semiconductor parameters and predict size quantization in unexplored materials. We highlighted this by demonstrating a statistically relevant difference in the band gap/size relation of wurtzite and zinc blende CdSe.

A semi-empirical QD sizing function

To establish a possible relation between the band gap E_1 and the diameter d for colloidal QDs, we expressed E_1 as an implicit function of d through the following relation:

$$E_1(d) = E_0 + F(E_1)f(d) \quad (1)$$

where E_0 represents the bulk optical band gap, *i.e.* the difference between the single-particle gap E_g and the exciton binding energy E_{ex} , $f(d)$ is a to-be-specified dimensionless function of the diameter that expresses the effect of size quantization, and $F(E_1)$ is a function with a unit of energy that corrects empirically the influence of non-parabolic energy bands on size quantization.

Since non-parabolic bands increasingly temper size quantization with decreasing size, we wrote $F(E_1)$ as a fixed fraction of the ratio between the bulk optical gap E_0 and the actual optical gap E_1 :

$$F(E_1) = E_{fit} \frac{E_0}{E_1(d)} \quad (2)$$

where E_{fit} is a fitting parameter with units of energy. Using Eqs 1 and 2, $E_1(d)$ can be written explicitly as:

$$E_1(d) = \frac{1}{2} \left[E_0 + \sqrt{E_0^2 + 4E_0E_{fit}f(d)} \right] \quad (3)$$

Finally, we developed an expression for the function $f(d)$ based on the considerations that (i) $E_1(d)$ should approach E_0 for large sizes, and (ii) $f(d)$ should describe strong quantization for parabolic bands for small sizes:

$$\begin{aligned} \lim_{d \rightarrow \infty} f(d) &= 0 \\ \lim_{d \rightarrow 0} f(d) &= \frac{d_0^2}{d^2} \end{aligned} \quad (4)$$

Moreover, (iii) by taking the exciton Bohr diameter d_0 as the size where $f(d)$ changes from large to small size behavior, we wrote $f(d)$ as:

$$f(d) = \frac{e^{-\frac{d}{d_0}}}{\left(1 - e^{-\frac{d}{d_0}}\right)^2} \quad (5)$$

Combining Eqs 3 and 5 then yields the relation between size and band gap that formed the starting point of this study:

$$E_1(d) = \frac{1}{2} \left[E_0 + \sqrt{E_0^2 + 4E_0 E_{fit} e^{-\frac{d}{d_0}} \left[1 - e^{-\frac{d}{d_0}}\right]^{-2}} \right] \quad (6)$$

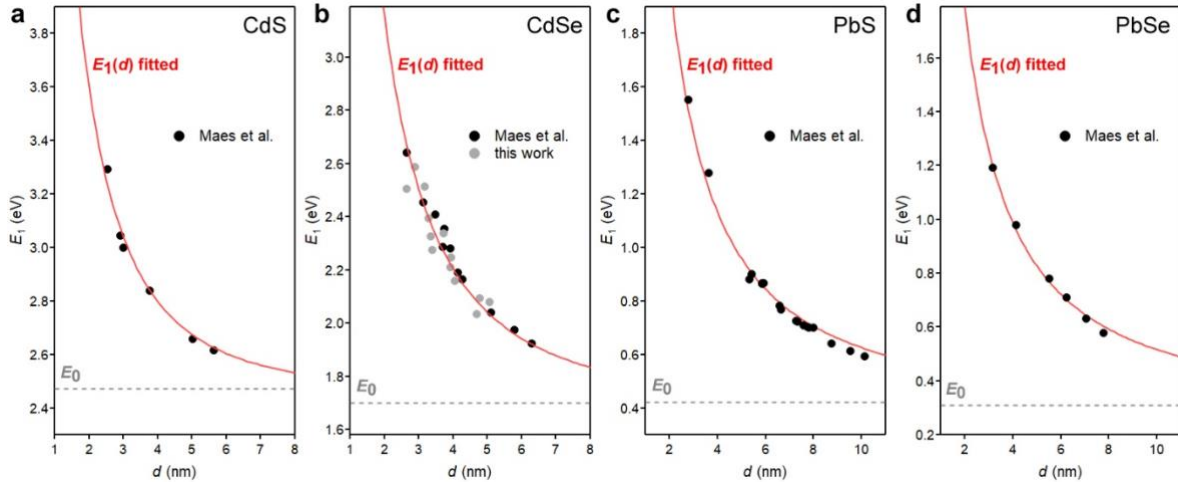


Figure 1. Optical band gap energy as function of SAXS diameter (full symbols) and respective fits using Eq 6 (continuous red line) for (a) CdS, (b) CdSe, (c) PbS and (d) PbSe QDs. Data for CdS, PbSe and PbS were obtained from Maes et al.¹⁰. Data for CdSe combine results from Maes et al.¹⁰ and the CdSe QDs analyzed in this work. The respective bulk optical band gaps are indicated with grey dashed lines.

We evaluated the suitability of Eq 6 to describe the band gap/size relation of QDs by fitting previously published datasets for CdS, CdSe, PbS and PbSe QDs (Figure 1). Sizes were obtained by small angle x-ray scattering (SAXS),¹⁰ which is a reliable and reproducible ensemble technique for sizing nanocrystals down to the nanometer length scale with little user-bias^{11,12}. Using known physical properties of the materials (Table 1), and considering E_{fit} as the only adjustable parameter of Eq 6, excellent fits to these datasets were obtained (Figure 1). For consistency, Bohr diameters d_0 were systematically calculated based on published effective masses and using the high-frequency dielectric constant ϵ_∞ of the material (Supporting Information, Section S2). Since quantization energies exceed typical phonon energies, we deemed ϵ_∞ more appropriate than the static ϵ_s to describe dielectric screening. However, as described later, the goodness of fit is independent of this choice.

Table 1. Physical parameters and fit results for the different materials analyzed by SAXS. Room temperature values of the parameters were used by default when available.

parameter	CdS	CdSe ^a	wz-CdSe	zb-CdSe	PbS	PbSe
E_g (eV)	2.501 ^{b,13}	1.713 ^c	1.751 ¹³	1.675 ¹³	0.42 ¹⁴	0.31 ¹⁴
E_{ex} (eV)	0.03 ^{b,13}	0.015 ^{b,13}	0.015 ¹³	0.015 ^{b,13}	$\ll E_g$	$\ll E_g$
E_0 (eV)	2.471	1.698	1.736	1.660	≈ 0.42	≈ 0.31
ϵ_∞	5.3 ¹³	6.2	6.2 ¹³	6.2 ¹³	17.4 ¹⁵	23.6 ¹⁵
d_0 (nm) ^d	3.1	5.9 ^c	5.2	6.6	45	113
E_{fit} (eV)	0.708	0.314	-	-	0.0152	0.0027

d_{fit} (nm)	3.5	6.8	5.4	7.7	54	82
----------------	-----	-----	-----	-----	----	----

^a results from fitting all CdSe data, including both polymorphs (Figure 1b).

^b reported value for wurtzite structure.

^c average between zinc blende and wurtzite values.

^d for d_0 determination, see Supporting Information, Section S2.

A Parameter-Free Prediction of Size Quantization

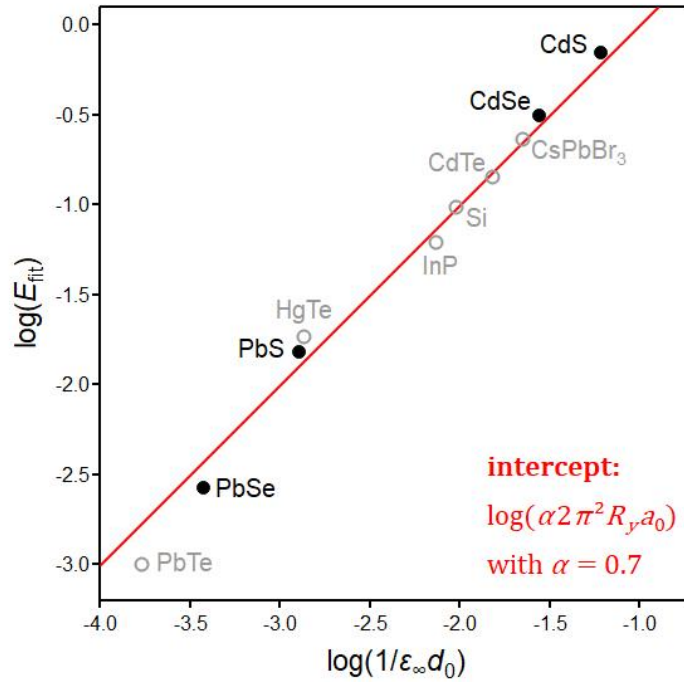


Figure 2. Log-log representation of E_{fit} as a function of $1/\epsilon_\infty d_0$. Values were obtained from the optimal fits, using Eq 6, of the reference data obtained for CdS, CdSe, PbS and PbSe QDs (filled black markers) and of the literature datasets for CdTe, PbTe, InP, Si, HgTe and CsPbBr₃ (open grey markers). The red line depicts the linear regression with $\alpha = 0.7$.

Considering the optimal values for E_{fit} for CdX and PbX listed in Table 1, it appears that larger Bohr diameters concur with smaller E_{fit} values. As outlined in Supporting Information, Section S3, an expression for E_{fit} can be obtained by using the sizing function for parabolic bands as a calibration reference, which indeed results in the anticipated $1/d_0$ scaling:

$$E_{fit} = \alpha 2 \pi^2 \frac{R_y a_0}{\epsilon_\infty d_0} \quad (7)$$

Here, R_y is the Rydberg unit of energy (13.606 eV) and a_0 is the Bohr radius of hydrogen (0.053 nm), while α is an adjustable parameter that compensates for approximations made in the calibration procedure. In view of Eq 7, Figure 2 represents E_{fit} as determined for CdS, CdSe, PbS and PbSe QDs (see Table 1) as a function of $1/\epsilon_\infty d_0$. One sees that a linear dependence is obtained over the more than two orders of magnitude spanned by the data, and a linear regression yields $\alpha = 0.7$, a result highlighting that a single, material-independent correction factor enables us to describe E_{fit} in terms of known material-dependent quantities.

With a single correction factor α , the combination of Eq 6 and 7 yields a parameter-free expression of the optical band gap as a function of E_0 , ϵ_∞ , and d_0 :

$$E_1(d) = \frac{1}{2} \left[E_0 + \sqrt{E_0^2 + 8E_0 \alpha \pi^2 \frac{R_y a_0}{\epsilon_\infty d_0} e^{-\frac{d}{d_0}} \left[1 - e^{-\frac{d}{d_0}} \right]^{-2}} \right] \quad (8)$$

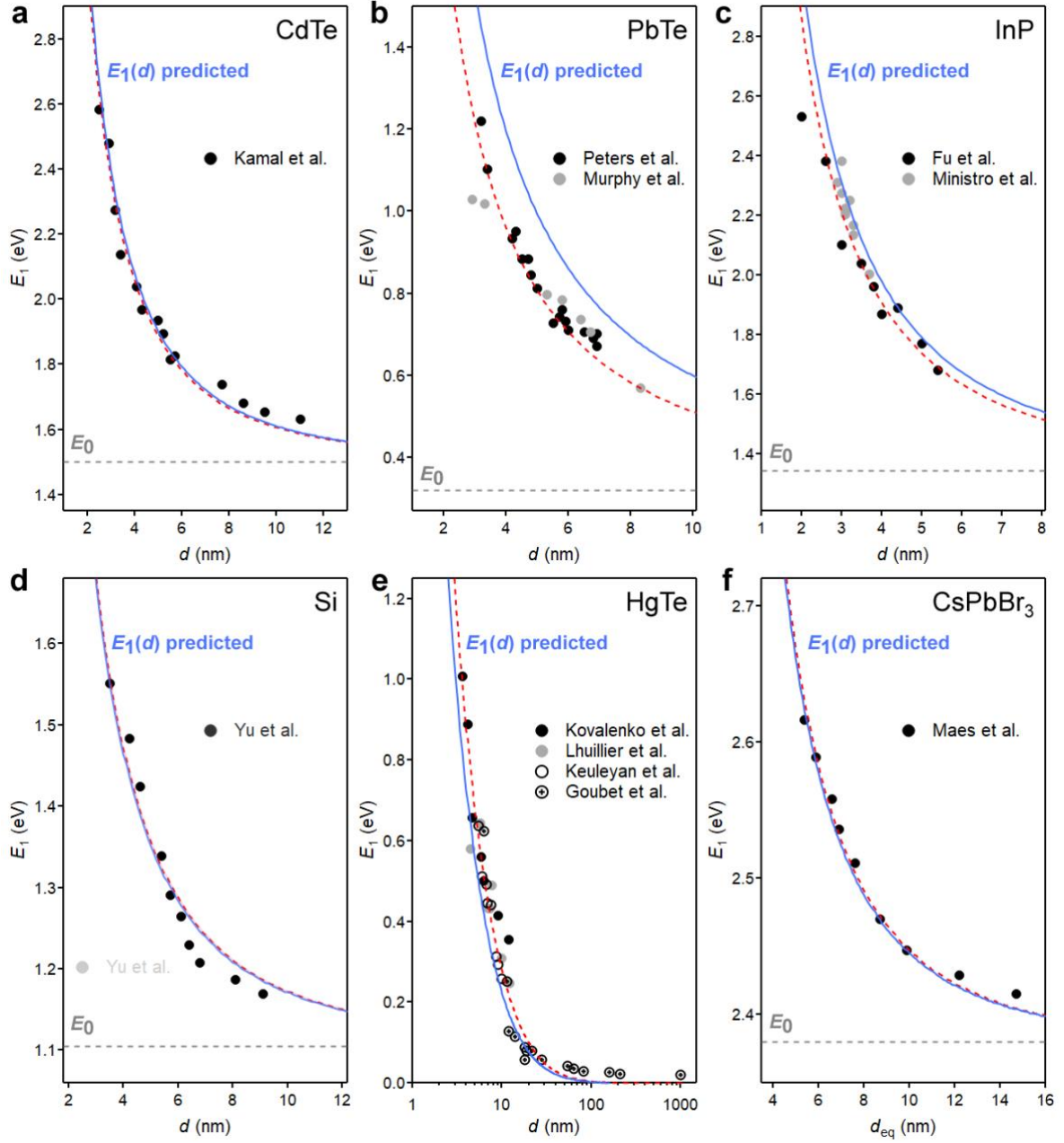


Figure 3. Optical band gap energy (blue continuous line) predicted by Eq 8 and (red dashed line) obtained as best fit of Eq 6 to the data (a) CdTe (dataset from Kamal et al.¹⁶), (b) PbTe (dataset from Peters et al. and Murphy et al.^{17,18}), (c) InP (dataset from Fu et al. and Ministro et al.^{19,20}), (d) Si (dataset from Yu et al.²¹), (e) HgTe (dataset from Kovalenko et al., Lhuillier et al., Keuleyan et al., and Goubet et al.²²⁻²⁵), and (f) CsPbBr₃ (dataset from Maes et al.²⁶) QDs. The respective bulk optical band gaps are indicated with grey dashed lines.

Eq 8 should predict the sizing curve of QDs without reference to experimental data. To test this hypothesis, we calculated the size-dependent optical gap using published data for the optical gap, effective masses and high frequency dielectric constants for 6 different semiconductors, and compared the outcome with size/band-gap datasets found in the literature. Figure 3 and Table 2 summarize these results.

We first completed the CdX and PbX families with CdTe and PbTe QDs, comparing predictions with datasets from Kamal et al.¹⁶ for CdTe, and from Peters et al.¹⁸ and Murphy et al.¹⁷ for PbTe. As shown in Figure 3a-b, agreement between prediction and experiment is almost perfect for CdTe. In the case of PbTe QDs, our theory underestimates sizes by 1-2 nm. Possibly, the correction for non-parabolic bands reaches a limit for this extreme case of a low effective mass, high ϵ_∞ material. Moving to InP, a III-V semiconductor that currently attracts high interest as a Cd-free material for display and lighting technologies, we again obtain excellent agreement with datasets for quasi-spherical QDs reported by Fu et al.¹⁹ and Micic et al.^{27,28}, and for yet unpublished data obtained from TEM analysis (see Supporting Information, Section S4)²⁰. Similar agreement was found in the case of Si QDs, an indirect-gap semiconductor for which we used the dataset published by Yu et al.²¹, see Figure 3d. In this case, the optical gap is retrieved from emission spectra, and we limited the comparison to the size range where emission efficiency is not affected by the nanocrystal size (i.e., $d > 3$ nm) as reported by the authors²¹.

To further test Eq 8 as a parameter-free expression for the optical band gap, we extended our study to HgTe QDs, for which the corresponding bulk semiconductor has a negative band gap, and CsPbBr₃ QDs with a cubic shape. In the case of HgTe, we adapted Eq 8 by (i) using the absolute value of the negative gap $|E_0|$ to determine deviations from non-parabolic behavior and (ii) realizing that the measured gap will extrapolate to 0 eV (see Supporting Information, Section S5). As a result, the optical gap of HgTe QDs is predicted by:

$$E_1(d) = \frac{1}{2} \left[E_0 + \sqrt{E_0^2 + 8|E_0| \alpha \pi^2 \frac{R_y a_0}{\epsilon_\infty d_0} e^{-\frac{d}{d_0}} \left[1 - e^{-\frac{d}{d_0}} \right]^{-2}} \right] \quad (9)$$

A very good agreement is obtained with size/band gap datasets from Kovalenko et al.²², Lhullier et al.²³, Keuleyan et al.²⁴, and Goubet et al.²⁵ (Figure 3e). The notation $|E_0|$ is used systematically hereafter for a generalized expression, suitable for both positive and negative band gap materials. For CsPbBr₃ QDs, we adjusted Eq 8 for the impact of shape on the confinement energy by comparing size quantization for parabolic bands in cubes with edge length L and spheres with diameter d . Setting $E_{Q,sphere} = 2\pi^2 \hbar^2 / md^2$ equal to $E_{Q,cube} = 3\pi^2 \hbar^2 / 2mL^2$, we can link the edge length to an equivalent diameter $d_{eq} = (2/\sqrt{3})L$. By interpreting d in Eq 8 as d_{eq} , we find an almost perfect agreement between the predicted optical gap and the optical gap of CsPbBr₃ cube-shaped QDs as reported by Maes et al.²⁶ (Figure 3f). The predictive power of Eq 8 may also be used to assess the properties of bulk semiconductors, and sort out diverging reported values for the same parameter. For instance, in Figure 3 for CsPbBr₃ we used the bulk optical band gap value ($E_0 = 2.38$ eV) reported by Mannino et al.²⁹, which was determined based on the critical point analysis method. This value gives particularly good predictions of the optical band gap whereas another value reported in earlier work³⁰ results in predictions that deviates significantly from the experimental dataset (see Supporting Information, Section S6).

Table 2. Physical parameters of different semiconductor materials tested for the predictive model and their respective E_{fit} and d_{fit} values. Room temperature values of the parameters were used by default when available.

parameter	CdTe	PbTe	InP	Si	HgTe	CsPbBr ₃
E_g (eV)	1.51 ¹³	0.32 ¹⁴	1.35 ¹⁴	1.12 ³¹	-	-
E_{ex} (eV)	0.010 ¹³	$\ll E_g$	0.005 ³²	0.015 ³³	-	-
E_0 (eV)	1.50	0.32	1.345	1.105	-0.32 ³⁴	2.38 ²⁹
ϵ_∞	7.1 ¹³	33.4 ¹⁵	9.5 ¹⁴	11.6 ¹⁴	14 ²³	7.3 ³⁵
d_0 (nm) ^a	9.3	175	14.3	9.0	53	6.1
E_{fit} (eV)	0.144	0.0010	0.0629	0.0975	0.0186	0.231
d_{fit} (nm)	8.9	103	12.3	9.2	73	6.3

^a see Supporting Information S2 for d_0 determination.

A generic sizing curve – the Bohr diameter as a fitting parameter

In spite of the very different nature of the tested materials, Figure 3 shows very good, if not perfect, agreements between the predicted and experimental optical band-gap energies. The sole significant deviations are observed for PbTe QDs, a material that may test the limits of the proposed correction for non-parabolicity. This consistency is underscored by fitting Eq 6 to the experimental datasets (Figure 3). The resulting E_{fit} values agree with the initial trend line derived from the CdX and PbX reference datasets, see Figure 2 and Table 2. Moreover, a linear fit to this extended dataset confirms the value of 0.7 for the correction coefficient α . We note that a similar pre-factor of 0.71 was previously calculated theoretically and implemented in the very first expression of size quantization in semiconductors by Efros et al.¹ to take into account the size dispersion of the nanocrystals based on a Lyfshitz-Slyosov size distribution. Alternatively, this factor could absorb deviations related to implicit approximation in our approach, see Supporting Information, Section S2.

Notwithstanding the potential of Eq 8 as a parameter-free size function, the bulk parameters the equation depends on are not always accurately known. This holds true in particular for the Bohr diameter d_0 . We estimated d_0 based on effective masses and the high frequency dielectric constant, which both have experimental uncertainties. For accurately sizing QDs starting from a measured optical gap, a further refinement of the Bohr diameter is therefore recommended. To this end, we adapted Eq 8 by replacing d_0 by an adjustable parameter d_{fit} , giving:

$$E_1(d) = \frac{1}{2} \left[E_0 + \sqrt{E_0^2 + 8|E_0| \alpha \pi^2 \frac{R_y a_0}{\epsilon_\infty d_{fit}} e^{-\frac{d}{d_{fit}}} \left[1 - e^{-\frac{d}{d_{fit}}} \right]^{-2}} \right] \quad (10)$$

Using the different experimental datasets, we adjusted d_{fit} to obtain the best interpolation using Eq 10 while keeping $\alpha = 0.7$, see Supporting Information, Section S7. As can be seen in Table 1 and 2, the optimal d_{fit} closely agrees with the calculated Bohr diameter for most datasets, a point confirming the good parameter-free prediction of optical gaps provided by Eq 8. Conveniently, Eq 10 can be re-expressed as a relation giving the diameter d as a function of the optical gap E_1 :

$$d(E_1) = d_{fit} \ln \frac{x(E_1) + 1}{x(E_1) - 1} \quad \text{with} \quad x(E_1) = \sqrt{1 + 2\epsilon_\infty d_{fit} \frac{E_1(E_1 - E_0)}{\alpha \pi^2 R_y a_0 |E_0|}} \quad (11)$$

Using the parameters listed in Tables 1 and 2, Eq 11 yields the QD diameter directly from the measured optical gap. For new materials without sufficient dataset to be fitted with Eq 10, one can still use Eq 11 to estimate the nanocrystal diameters from the measured optical band gap by replacing d_{fit} with reported or calculated d_0 values based on effective masses and the high frequency dielectric constant.

A particular aspect of the analysis presented here, is that predictions using Eq 8 or fittings using Eq 10 consistently relies on the high frequency dielectric constant. Interestingly, highly similar results are obtained when using the static dielectric constants throughout, see Supporting Information, Section S8. This outcome can be understood by considering Eq 8 in the limit of strong size quantization ($d \ll d_0$), which yields a limiting expression independent of the dielectric constant. Hence, our approach does not settle the debate on what dielectric constant – static or high-frequency – is appropriate to calculate exciton Bohr diameters in QDs but consistent combinations of dielectric constant and Bohr radius are used to predict optical gaps using Eq 8.

Optical gap analysis - zinc blende and wurtzite CdSe

A model function that relies on a single fitting parameter does not have any redundant parameter. This greatly facilitates the analysis of statistically relevant differences between datasets. We used this aspect of Eq 10 to assess possible subtle differences in sizing behavior related to the two different polymorphs of CdSe: zinc blende and wurtzite. It is well known that both cubic zinc blende (zb-CdSe) or a hexagonal wurtzite (wz-CdSe) CdSe can be formed by colloidal synthesis. However, due to small crystallite sizes, discriminating zb-CdSe from wz-CdSe QDs using powder X-ray diffraction (XRD) is not straightforward³⁶. Moreover, both polymorphs may coexist in the same QD sample and single CdSe QDs may show zinc blende/wurtzite stacking faults³⁷. To obtain a well-defined band gap/size dataset for both polymorphs, we therefore synthesized several CdSe QD samples using synthesis protocols^{38,39}, known to produce rather pure crystal phases (see experimental section for synthesis details). For both synthesis methods, we prepared a series of CdSe QDs with optical band-gaps ranging from 2.0 to 2.6 eV, see Figure 4a,b. Representative TEM micrographs and XRD patterns of these samples are provided in Supporting Information, Section S9.

Interestingly, zb- and wz-CdSe QDs feature markedly different absorption spectra. In particular, the energy separation between the second and first excitonic transitions (E_2-E_1) is larger for zb-CdSe than for wz-CdSe QDs^{37,40,41}. We determined this splitting energy for all CdSe samples, and obtained two distinct trend lines that enabled us to classify each sample as zb- or wz-CdSe (Figure 4c). For completeness, we also report in Figure 4c data corresponding to the CdSe reference set we used in Figure 1¹⁰. In this case, the E_2-E_1 trend suggests that these QDs consist of a mixture of zb-CdSe and wz-CdSe rather than pure zb-CdSe, as was originally stated. This is consistent with the use of amine and phosphine reactants in that synthesis⁴², which may have resulted in some wz-CdSe fraction as well^{40,43}.

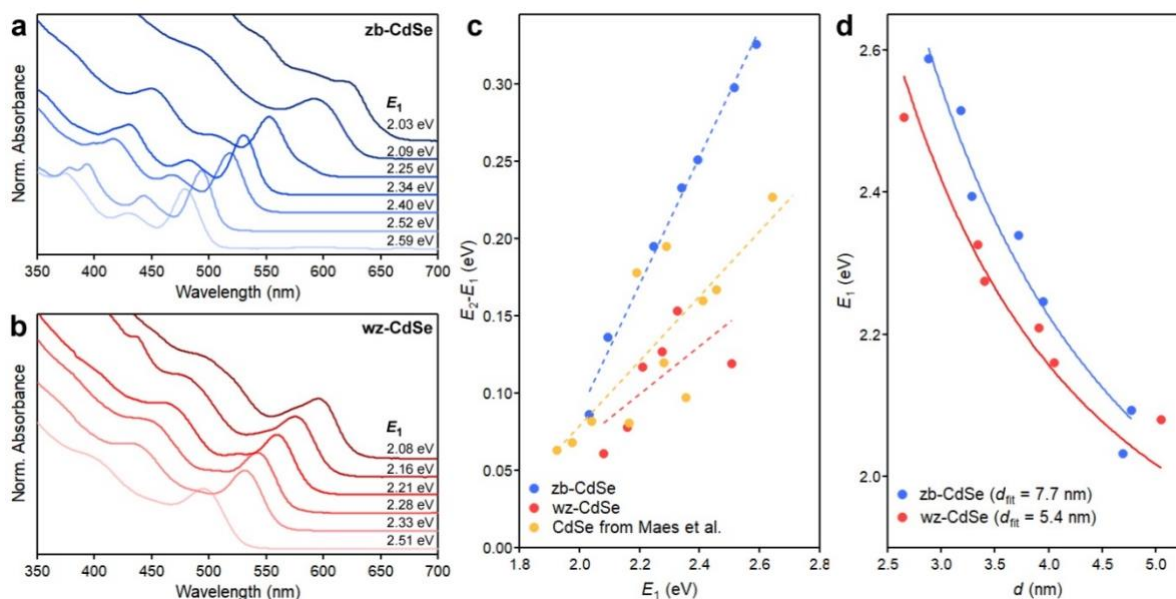


Figure 4. Absorption spectra of (a) zb-CdSe QDs and (b) wz-CdSe QDs. (c) Energy difference between the first and second excitonic transitions (E_2-E_1) as a function of the first transition energy (E_1) for zb-CdSe and wz-CdSe QD sets synthesized for this study and compared to the CdSe QD set synthesized in a previous study (Maes et al.¹⁰). (d) Optical band gap energy as a function of QD diameter, and fitted with Eq 10.

We determined the average diameters of the different CdSe QDs using SAXS, see Supporting Information, Section S9, and fitted the resulting band gap/size data using Eq 10 for zb-CdSe and wz-CdSe QDs separately, see Figure 4d. Using their respective bulk electronic band gaps and a common bulk exciton binding energy of 0.015 eV,¹³ we obtained two different curves with d_{fit} values of 7.7 nm and 5.4 nm for zb- and wz-CdSe, respectively. A statistical analysis reveals that the probability for these two distributions to be random variations around a common curve is below 1% (Supporting Information, Section S9). This evaluation confirms the statistical significance of the two distinct d_{fit} values, and is in line with zb- and wz-CdSe having a different Bohr radius.

In the size range 2.5-5 nm ($E_1 = 2.1-2.8$ eV), which covers most of the potential applications and interests for CdSe QDs, this difference translates in zb-CdSe QDs being about 0.3 nm larger than wz-QDs for a given optical gap. This difference can have a significant impact on, for example, concentration determinations. Even so, a single generic sizing curve for CdSe QDs can be more relevant in practice given the difficulty to determine the actual crystal structure of CdSe QDs, the high likelihood of obtaining mixed polymorphs and the albeit small difference in size between the polymorphs. To this end, we fitted the complete dataset of CdSe QDs using the average between zinc blende and wurtzite values for the bulk electronic band gap, $E_g = 1.713$ eV. The outcome is a single d_{fit} value, reported in Table 1.

Based on the experimental sizing curves, we analyzed optical band gaps in zb- and wz-CdSe QDs within the effective mass calculations,⁴⁴ for which we examined different sets of Luttinger parameters, see Supporting Information, Section S10. By comparing the experimental and calculated energy separation between the first and second excitonic transition, we find that sets of Luttinger parameters from refs.^{45,46} and ref.⁴⁷ are optimal for zb-CdSe and wz-CdSe QDs, respectively. Given these theoretical calculations, we can assess the difference in the absorbance spectra of the two polymorphs. As shown in Figure 4d, the optical gap of zb-CdSe QDs in the size range 2.5-5.0 nm is at higher energy than wz-QDs, even if bulk zb-CdSe has the smaller band gap. From fitting the experimental data, see Supporting Information, Section S10, we find that this large blueshift comes from stronger quantization of both the electron and hole in zb-CdSe. The second absorption feature then corresponds to an exciton formed by the electron ground state and the second S-type hole state. This difference is controlled by the separation between the 1S and 2S hole states, which is larger for zb-CdSe than for wz-CdSe QDs^{37,40}, in line with the experimental observations (Figure 4d).

Conclusion

In conclusion, through a proportional correction for non-parabolic energy bands, this work establishes a generic sizing function for fitting experimental band-gap/size datasets and predicting size quantization based on known bulk semiconductor parameters. Using a single, physically meaningful parameter and allowing for extrapolation, this sizing function provides a sound, unified basis for QD size calibration. Moreover, researchers may well use the predictive power of the sizing function to assess bulk semiconductor constants, explore size quantization in new materials or structures or, as we show here, refine band-structure parameters. In this way, this work will help making the wealth of data assembled over the last tens of years on various colloidal semiconductor QDs useful and accessible for the broader field of materials physics.

Experimental section

zb-CdSe QDs synthesis. The CdSe QDs with predominantly zinc blende structure were synthesized according to a procedure based on the injection of undissolved Se powder into a hot mixture of cadmium carboxylate in octadecene (ODE)³⁸. Briefly, CdO (0.5-1 mmol) is dissolved with a fatty acid (3 Cd equivalent) in ODE (10 mL) at 260 °C under air atmosphere. A solution of undissolved Se powder (0.1 Cd equivalent) in ODE (1 mL) is injected rapidly and the reaction is left to proceed for 5 min. The QDs are then purified by repeated centrifugation, using toluene and methanol as solvent and non-solvent, respectively. For this high chemical yield synthesis, the size of the QDs was varied by changing the length of the fatty acid from nonanoic acid to behenic acid, with longer acid chains yielding smaller nanocrystals, and/or the overall concentration of the synthesis, with higher concentrations yielding larger nanocrystals³⁸. After synthesis, the surface ligands were systematically exchanged for oleic acid.

wz-CdSe QDs synthesis. The CdSe QDs with predominantly wurtzite structure were synthesized according to a procedure initially reported by Carbone et al.³⁹, which was greatly popularized for the seeded growth of CdSe/CdS dot-in-rods thanks to the non-centrosymmetric structure of these core QDs. The synthesis was later adapted to prevent the formation of phosphonic anhydrides, and the

subsequent aggregation of QDs at room temperature, by adding a long chain alcohol to the synthesis⁴⁸. In a typical synthesis, CdO (1.5 mmol) is dissolved with tetradecylphosphonic acid (6 mmol) in a degassed mixture of oleyl alcohol (24 mmol) and trioctylphosphine oxide (10 g) at 350 °C under nitrogen. Solutions of trioctylphosphine (TOP, 2 ml), followed by TOP-Se (1.7 M, 1.5 ml, Se fully dissolved beforehand at 60 °C in a glove box), are injected rapidly in the reaction mixture under nitrogen. In this case, the size of the QDs was adjusted by varying the reaction time from a couple of seconds only, for the smallest ones, to several tens of seconds for the larger ones. The QDs are finally purified by repeated centrifugation, using toluene and methanol as solvent and non-solvent, respectively.

Materials characterization. The UV-vis absorption spectra of the QDs were measured in toluene using a PerkinElmer Lambda 950 spectrometer. For XRD analyses, the QD solutions were drop-casted on a piece of cover glass slide and the diffraction patterns were measured with a Thermo Scientific ARL X'Tra diffractometer, operated at 40 kV/30 mA, using Cu-K α radiation and a Peltier cooled Si(Li) solid-state detector. The diffraction patterns were acquired over a 5-110° 2 θ range with a 0.02° step and 2.5° soller slits on both incident and receiving sides for higher resolution. TEM images were acquired with a Cs-corrected JEOL 2200FS microscope operated at 200 kV. The SAXS experiments were performed on the ID02 beamline⁴⁹ of the ESRF (European Synchrotron Radiation Facility) at an energy of 12.23 keV and a sample to detector distance of 1m. The QD samples were inserted as toluene dispersions in a glass capillary. The data analysis was performed as previously reported for the size analysis of nanocrystals in the case of glass capillaries¹⁰.

Acknowledgments

ZH and AR acknowledge the bilateral FWO-Vlaanderen and Russian Science Foundation research cooperation (FWO grant No. G0F0920N) for funding. AR and AG acknowledge the Russian Science Foundation (Grant No. 20-42-01008). AG acknowledges support of the Grants Council of the President of the Russian Federation. The SAXS analyses were performed as part of a project that has received funding from the European Research Council (ERC) under the European Union's Horizon 2020 research and innovation program (Grant agreement No. 865995).

References

- 1 Efros, A. L. & Efros, A. L. Interband absorption of light in a semiconductor sphere. *Sov. Phys. Semicond.* **16**, 772, (1982).
- 2 Brus, L. E. A simple model for the ionization potential, electron affinity, and aqueous redox potentials of small semiconductor crystallites. *J. Chem. Phys.* **79**, 5566-5571, (1983).
- 3 Efros, A. L. & Brus, L. E. Nanocrystal Quantum Dots: From Discovery to Modern Development. *ACS Nano* **15**, 6192-6210, (2021).
- 4 Yu, W. W., Qu, L., Guo, W. & Peng, X. Experimental Determination of the Extinction Coefficient of CdTe, CdSe, and CdS Nanocrystals. *Chem. Mater.* **15**, 2854-2860, (2003).
- 5 Jasieniak, J., Smith, L., Embden, J. v., Mulvaney, P. & Califano, M. Re-examination of the Size-Dependent Absorption Properties of CdSe Quantum Dots. *J. Phys. Chem. C* **113**, 19468-19474, (2009).
- 6 de Mello Donegá, C. & Koole, R. Size Dependence of the Spontaneous Emission Rate and Absorption Cross Section of CdSe and CdTe Quantum Dots. *J. Phys. Chem. C* **113**, 6511-6520, (2009).
- 7 Čapek, R. K. *et al.* Optical Properties of Zincblende Cadmium Selenide Quantum Dots. *J. Phys. Chem. C* **114**, 6371-6376, (2010).
- 8 Moreels, I. *et al.* Composition and Size-Dependent Extinction Coefficient of Colloidal PbSe Quantum Dots. *Chem. Mater.* **19**, 6101-6106, (2007).

- 9 Moreels, I. *et al.* Size-Dependent Optical Properties of Colloidal PbS Quantum Dots. *ACS Nano* **3**, 3023-3030, (2009).
- 10 Maes, J. *et al.* Size and Concentration Determination of Colloidal Nanocrystals by Small-Angle X-ray Scattering. *Chem. Mater.* **30**, 3952-3962, (2018).
- 11 Li, T., Senesi, A. J. & Lee, B. Small Angle X-ray Scattering for Nanoparticle Research. *Chem. Rev.* **116**, 11128-11180, (2016).
- 12 Pauw, B. R., Kastner, C. & Thunemann, A. F. Nanoparticle size distribution quantification: results of a small-angle X-ray scattering inter-laboratory comparison. *J. Appl. Crystallogr.* **50**, 1280-1288, (2017).
- 13 Adachi, S. *Handbook on Physical Properties of Semiconductors*. Vol. Volume 3: II–VI Compound Semiconductors (Springer US, 2004).
- 14 Adachi, S. *Optical Constants of Crystalline and Amorphous Semiconductors* Vol. Numerical Data and Graphical Information (Springer US, 1999).
- 15 Zemel, J. N., Jensen, J. D. & Schoolar, R. B. Electrical and Optical Properties of Epitaxial Films of PbS, PbSe, PbTe, and SnTe. *Phys. Rev.* **140**, A330-A342, (1965).
- 16 Kamal, J. S. *et al.* Size-Dependent Optical Properties of Zinc Blende Cadmium Telluride Quantum Dots. *J. Phys. Chem. C* **116**, 5049-5054, (2012).
- 17 Murphy, J. E. *et al.* PbTe Colloidal Nanocrystals: Synthesis, Characterization, and Multiple Exciton Generation. *J. Am. Chem. Soc.* **128**, 3241-3247, (2006).
- 18 Peters, J. L., de Wit, J. & Vanmaekelbergh, D. Sizing Curve, Absorption Coefficient, Surface Chemistry, and Aliphatic Chain Structure of PbTe Nanocrystals. *Chem. Mater.* **31**, 1672-1680, (2019).
- 19 Fu, H. & Zunger, A. InP quantum dots: Electronic structure, surface effects, and the redshifted emission. *Phys. Rev. B* **56**, 1496-1508, (1997).
- 20 Ministro, J. & Hens, Z. *A study on the synthesis and the optical properties of InP-based quantum dots* Master of Science in Chemistry thesis, Ghent University, (2014), <<http://lib.ugent.be/catalog/rug01:002163550>>.
- 21 Yu, Y. *et al.* Size-Dependent Photoluminescence Efficiency of Silicon Nanocrystal Quantum Dots. *J. Phys. Chem. C* **121**, 23240-23248, (2017).
- 22 Kovalenko, M. V. *et al.* Colloidal HgTe Nanocrystals with Widely Tunable Narrow Band Gap Energies: From Telecommunications to Molecular Vibrations. *J. Am. Chem. Soc.* **128**, 3516-3517, (2006).
- 23 Lhuillier, E., Keuleyan, S. & Guyot-Sionnest, P. Optical properties of HgTe colloidal quantum dots. *Nanotechnology* **23**, 175705, (2012).
- 24 Keuleyan, S. E., Guyot-Sionnest, P., Delerue, C. & Allan, G. Mercury Telluride Colloidal Quantum Dots: Electronic Structure, Size-Dependent Spectra, and Photocurrent Detection up to 12 μm . *ACS Nano* **8**, 8676-8682, (2014).
- 25 Goubet, N. *et al.* Terahertz HgTe Nanocrystals: Beyond Confinement. *J. Am. Chem. Soc.* **140**, 5033-5036, (2018).
- 26 Maes, J. *et al.* Light Absorption Coefficient of CsPbBr₃ Perovskite Nanocrystals. *J. Phys. Chem. Lett.* **9**, 3093-3097, (2018).
- 27 Micic, O. I., Curtis, C. J., Jones, K. M., Sprague, J. R. & Nozik, A. J. Synthesis and Characterization of InP Quantum Dots. *J. Phys. Chem.* **98**, 4966-4969, (1994).
- 28 Mičić, O. I., Sprague, J., Lu, Z. & Nozik, A. J. Highly efficient band-edge emission from InP quantum dots. *Appl. Phys. Lett.* **68**, 3150-3152, (1996).
- 29 Mannino, G. *et al.* Temperature-Dependent Optical Band Gap in CsPbBr₃, MAPbBr₃, and FAPbBr₃ Single Crystals. *J. Phys. Chem. Lett.* **11**, 2490-2496, (2020).
- 30 Dirin, D. N., Cherniukh, I., Yakunin, S., Shynkarenko, Y. & Kovalenko, M. V. Solution-Grown CsPbBr₃ Perovskite Single Crystals for Photon Detection. *Chem. Mater.* **28**, 8470-8474, (2016).
- 31 Barbagioanni, E. G., Lockwood, D. J., Simpson, P. J. & Goncharova, L. V. Quantum confinement in Si and Ge nanostructures. *J. Appl. Phys.* **111**, 034307, (2012).

- 32 Mathieu, H., Chen, Y., Camassel, J., Allegre, J. & Robertson, D. S. Excitons and polaritons in InP. *Phys. Rev. B* **32**, 4042-4051, (1985).
- 33 Green, M. A. Improved value for the silicon free exciton binding energy. *AIP Adv.* **3**, 112104, (2013).
- 34 Orłowski, N., Augustin, J., Gołacki, Z., Janowitz, C. & Manzke, R. Direct evidence for the inverted band structure of HgTe. *Phys. Rev. B* **61**, R5058-R5061, (2000).
- 35 Yang, Z. *et al.* Impact of the Halide Cage on the Electronic Properties of Fully Inorganic Cesium Lead Halide Perovskites. *ACS Energy Lett.* **2**, 1621-1627, (2017).
- 36 Murray, C. B., Norris, D. J. & Bawendi, M. G. Synthesis and characterization of nearly monodisperse CdE (E = sulfur, selenium, tellurium) semiconductor nanocrystallites. *J. Am. Chem. Soc.* **115**, 8706-8715, (1993).
- 37 Wu, F. *et al.* Fine-tuning the crystal structure of CdSe quantum dots by varying the dynamic characteristics of primary alkylamine ligands. *CrystEngComm* **20**, 4492-4498, (2018).
- 38 Flamee, S. *et al.* Fast, High Yield, and High Solid Loading Synthesis of Metal Selenide Nanocrystals. *Chem. Mater.* **25**, 2476-2483, (2013).
- 39 Carbone, L. *et al.* Synthesis and Micrometer-Scale Assembly of Colloidal CdSe/CdS Nanorods Prepared by a Seeded Growth Approach. *Nano Lett.* **7**, 2942-2950, (2007).
- 40 Mahler, B., Lequeux, N. & Dubertret, B. Ligand-Controlled Polytypism of Thick-Shell CdSe/CdS Nanocrystals. *J. Am. Chem. Soc.* **132**, 953-959, (2010).
- 41 Mohamed, M. B., Tonti, D., Al-Salman, A., Chemseddine, A. & Chergui, M. Synthesis of High Quality Zinc Blende CdSe Nanocrystals. *J. Phys. Chem. B* **109**, 10533-10537, (2005).
- 42 Čapek, R. K. *et al.* Synthesis of Extremely Small CdSe and Bright Blue Luminescent CdSe/ZnS Nanoparticles by a Prefocused Hot-Injection Approach. *Chem. Mater.* **21**, 1743-1749, (2009).
- 43 Gao, Y. & Peng, X. Crystal Structure Control of CdSe Nanocrystals in Growth and Nucleation: Dominating Effects of Surface versus Interior Structure. *J. Am. Chem. Soc.* **136**, 6724-6732, (2014).
- 44 Ekimov, A. I. *et al.* Absorption and intensity-dependent photoluminescence measurements on CdSe quantum dots: assignment of the first electronic transitions. *J. Opt. Soc. Am. B* **10**, 100-107, (1993).
- 45 Norris, D. J. & Bawendi, M. G. Measurement and assignment of the size-dependent optical spectrum in CdSe quantum dots. *Phys. Rev. B* **53**, 16338-16346, (1996).
- 46 Fu, H., Wang, L.-W. & Zunger, A. Applicability of the k.p method to the electronic structure of quantum dots. *Phys. Rev. B* **57**, 9971-9987, (1998).
- 47 Richard, T., Lefebvre, P., Mathieu, H. & Allègre, J. Effects of finite spin-orbit splitting on optical properties of spherical semiconductor quantum dots. *Phys. Rev. B* **53**, 7287-7298, (1996).
- 48 Drijvers, E. *et al.* Revisited Wurtzite CdSe Synthesis: A Gateway for the Versatile Flash Synthesis of Multishell Quantum Dots and Rods. *Chem. Mater.* **28**, 7311-7323, (2016).
- 49 Narayanan, T. *et al.* A multipurpose instrument for time-resolved ultra-small-angle and coherent X-ray scattering. *J. Appl. Crystallogr.* **51**, 1511-1524, (2018).